Journal of Nuclear Medicine, published on September 29, 2016 as doi:10.2967/jnumed.116.178327

Cure of human ovarian carcinoma solid xenografts by fractionated [211At] alpha-radioimmunotherapy: Influence of tumor absorbed dose and effect on long-term survival

Tom Bäck[1*], Nicolas Chouin[2], Sture Lindegren[1], Helena Kahu[3], Holger Jensen[4], Per Albertsson[3] and Stig Palm[1]

Departments of [1]Radiation Physics and [3]Oncology, Sahlgrenska Academy, University of Gothenburg, Gothenburg, Sweden

[2]LUNAM Université, Oniris, AMaROC , Nantes, France

[4] PET and Cyclotron Unit, Department of Clinical Physiology and Nuclear Medicine, Copenhagen University Hospital, Copenhagen, Denmark

*Corresponding and First author:
Tom Bäck
Department of Radiation Physics, University of Gothenburg
Gula stråket 2B
SE-413 45 Gothenburg, Sweden
tom.back@radfys.gu.se
+46 70 697 4058

Running title: Cure of solid xenografts by alpha-RIT

Word count: 5103

ABSTRACT

The goal of this study was to investigate if targeted alpha therapy (TAT) could be used to successfully treat also macro tumors, in addition to its established role for treating micrometastatic and minimal disease. We used an intravenous fractionated regimen of alpha-radioimmunotherapy (α-RIT) in a subcutaneous tumor model in mice. We aimed at evaluating the absorbed dose levels required for tumor eradication and to monitor tumor growth, as well as the long-term survival after treatment.

Methods

Mice bearing subcutaneous tumors (50 mm^3, NIH:OVCAR-3) were injected repeatedly (1 to 3 intravenous injections, 7-10 days apart allowing bone-marrow recovery) with ^{211}At-MX35-F(ab')$_2$ at different activities (close to acute myelotoxicity). Mean absorbed dose to tumors and organs were estimated from biodistribution data and summed for the fractions. Tumor growth was monitored for 100 days and survival for 1 year after treatment. Toxicity analysis included body weight, white blood cell count (WBC) and hematocrit.

Results

Effects on tumor growth following fractionated α-RIT with ^{211}At-MX35-F(ab')$_2$ was strong and dose-dependent. Complete remission (tumor free fraction, TFF=100%) was found for tumor doses of 12.4 and 16.4 Gy. The administered activities were high and long-term toxicity effects (up to 60 weeks) were clear. Above 1 MBq, the median survival decreased linearly with injected activity, from 44 to 11 weeks. Toxicity was also seen by reduced body weight. WBC-analysis after α-RIT indicated bone marrow recovery for the low activity groups, while for high activity groups the reduction was close to acute myelotoxicity. A decrease in hematocrit was seen at a late interval (34-59 weeks after therapy). The main external indication of poor health was dehydration.

Conclusion

Having observed complete eradication of solid tumor xenografts, we conclude that TAT regimens could stretch beyond the realm of micrometastatic disease and be eradicative also for macro tumors. Our observations indicated that at least 10 Gy is required. This was in good agreement with the calculated tumor control probability (TCP). Considering a relative biological effectiveness (RBE) of 5, this dose level seemed reasonable. However, complete remission was achieved first at activity levels close-to lethal and was accompanied with biological effects that reduced the long-term survival.

Key words: Targeted alpha therapy, radioimmunotherapy, alpha-particles, astatine-211, dosimetry

INTRODUCTION

Radioimmunotherapy has long been seen as promising for therapy of various cancers, but its use in clinical practice has been limited. The main obstacle for greater success has been the tumor-to-normal tissue absorbed dose ratios, where only low or moderate levels have been reached, meaning that the activity amounts needed for tumors eradication could not be used due to the increased normal tissue toxicity.

Most studies exploring radioimmunotherapy have used beta-emitting radionuclides but also α-particle emitting radionuclides have been proposed, i.e. alpha-radioimmunotherapy (α-RIT). Alpha particles have much shorter range (50–100 μm) and higher linear energy transfer (~100 keV/μm) than beta particles, resulting in much higher tumor-to-normal tissue absorbed dose ratios for isolated single cancer cells or small cell clusters(*1*), such as micrometastases. Alpha-emitters have therefore been studied, and proven successful experimentally, for therapy of microscopic tumors (*2-11*).

For irradiation of larger tumors, α-emitters do not have the same obvious advantages over beta-emitters. Instead, the short path length of α-particles is likely a disadvantage. The antibody uptake in solid tumors has been shown to be decreasing with increasing tumor mass (*12*), e.g. due to elevated interstitial pressure, poor vascularization, and necrosis. In addition, the activity distribution within tumors is often heterogeneous due to poor diffusion of the antibody. The use of short-ranged α-emitters may therefore result in some fraction of the tumor cells receiving very low absorbed dose. For the longer-ranged beta-emitters, e.g. ^{90}Y, such obstacles might be partially compensated for by the cross-fire effect.

There may, however, be a rationale for using α-emitters in treatments also of macro-tumors. This could involve clinical situations where tumors at a spectrum of sizes, ranging from single cells to millimeter-sized nodules, can be expected to occur. In addition to the favorable tumor-to-normal tissue absorbed dose ratios for microtumors, the radiobiological effects of α-particles may make them favorable over β-particles also for solid tumors, e.g. due to the induction of bystander effects (*13*). The rationale for using α-emitters in treatments of macro-tumors may also arise with new regimens, e.g. pretargeted α-RIT (*14*), by which higher tumor-to-normal tissue absorbed dose ratios and more uniform tumor uptake can be achieved.

We have previously used ^{211}At-MX35-F(ab')$_2$ in a subcutaneous macroscopic tumor model to derive the relative biological effectiveness (RBE) of α-RIT *in vivo* (*15*). Single intravenous administrations at different activities provided a range of absorbed doses to tumors, which were monitored for growth. The study showed a dose-dependent inhibition of growth, with the greatest delay seen for the highest tumor doses (2.7 and 4.1 Gy). However, all tumors resumed exponential growth and the anti-tumor effect of higher administered activity could not be evaluated due to bone-marrow toxicity.

The aim of the present study was to investigate if macro-tumors could be completely eradicated by fractionated α-RIT and, if so, to determine the required tumor absorbed dose. The aim was also to

evaluate the corresponding long-term toxicity. We used the subcutaneous tumor model, with 1–3 injections of ^{211}At-MX35 F(ab´)$_2$ administered 7-10 days apart. Tumor growth was monitored by volume measurements for up to 100 days and the long-term toxicity up to 60 weeks. Absorbed doses to tumors and normal tissues were calculated from previous biodistribution data, complemented by new data on the influence on tumor uptake from a prior α-RIT fraction.

MATERIALS AND METHODS

Radioimmunoconjugate

Astatine-211 ($t_{½}$ = 7.2 h) was produced at the PET and Cyclotron Unit at Copenhagen University Hospital (Copenhagen, Denmark). The F(ab´)$_2$ fragment of the monoclonal antibody MX35, was produced by Strategic BioSolutions (Newark, USA), and kindly provided by the Memorial Sloan-Kettering Cancer Center (New York). The MX35 is directed to the sodium-dependent phosphate-transport protein 2b (NaPi2b) (*16*) expressed on ~90% of human epithelial ovarian cancers . Isolation of ^{211}At, radiolabeling and immunoreactivity analysis was performed as previously described (*15,17,18*).

Tumor model and assessment of therapy

The animals in the current study were also used as a cohort in a previously published study assessing long-term renal toxicity following α-RIT (*19*). Using the human ovarian cancer cell line NIH:OVCAR-3 (obtained from American Type Culture Collection and cultured at 37°C in RPMI 1640 medium supplemented with 10% fetal calf serum, 2 mM L-glutamine and 1% penicillin-streptomycin), two subcutaneous xenografts were established in the scapula region of each female nude mouse (BALB/c *nu/nu*, 4–8 weeks, Charles River, Kisslegg, Germany) by inoculation of 2 x 10^7 cells (in 0.4 mL PBS).

At 6–12 days after cell inoculation (tumor volumes approximately 50 mm^3) α-RIT was given by tail vein injection of ^{211}At-MX35-F(ab')$_2$ (range 0.36–1.53 MBq). Controls received unlabeled MX35-F(ab')$_2$ only. Divided in 12 groups (8–10 animals per group), 4 groups received a single treatment, 8 groups received a second treatment after 7 days and 4 groups also a third treatment, another 7 days later (Table 1).

The tumor volumes (V) were monitored by slide caliper measurements of the larger tumor diameter (D_L) and its perpendicular diameter (D_P), using the formula (*20*): $V = (D_L \times D_P^2)/2$. When D_L exceeded 15 mm, or at signs of ulcerated skin, the tumors were surgically removed using Isoflurane (Baxter Healthcare Corporation, Illinois, USA) for anesthesia and Temgesic (RB Pharmaceuticals Limited, Berkshire, UK) for sedation. After suture, the animals were monitored for recovery and body temperature was assisted. Animals with tumor relapse were operated a second time. If later presented with yet another relapse, they were taken out of the study (and assigned as censored in the survival analysis).

Eighty days after tumor cell inoculation the tumor free fraction (TFF) was calculated by dividing the number of eradicated tumor by the initial number of tumors in each group. Tumors not viably established (volume <25 mm^3) at first therapy were excluded from the analysis.

Blood sampled from tail vein were analyzed for erythrocytes (hematocrit) and white blood cell count (WBC). Hematocrit was monitored repeatedly over time. The WBC was measured 5–7 days after α-RIT (representing nadir) and at 10–12 days (representing recovery). Blood samples (10 μL) from 3–5 animals per group were analyzed using a microcell counter (Sysmex F-820, Sysmex Corporation, Kobe, Japan). Late-term WBC was analyzed in one animal per low-activity group (groups 6, 7, 9, 10 and 11) at one year (37–49 weeks) after α-RIT.

Body weight and health status were monitored weekly to study termination (60 weeks). Animals were sacrificed on sign of poor health, e.g. dehydration, abnormal behavior or low weight progression. The study was approved by the local Ethics Committee and all animals were maintained according to the national Animal Welfare Agency's regulations.

Dosimetry

Mean absorbed dose to tumors and normal tissues was calculated from biodistribution data previously published for single ^{211}At-MX35-F(ab')$_2$ administration (*15*). These data were complemented by a new biodistribution study to determine the uptake (%IA/g) on tumors that had previously been treated with α-RIT. Nine tumor carrying mice were administered 1.5 MBq ^{211}At-MX35-F(ab')$_2$ and 14 days later the biodistribution at 1, 9, and 21 hpi (3 mice, i.e. 6 tumors per time-point) following repeat α-RIT was determined.

Tissue activity concentrations at different times after injection were measured using a γ-counter (Wizard 1480, PerkinElmer Life Sciences) and the cumulated activity concentration, $\widetilde{C}$ (total number of decays/kg) was calculated from time-activity plots up to 48 hpi. The mean absorbed dose, D, was calculated from the formula:

$$D = \widetilde{C} \cdot \Delta \cdot \emptyset$$

using a mean α-particle energy (Δ) of 1.09 x 10^{-12} J per ^{211}At decay (neglecting contribution from photons and electrons) and an absorbed fraction, $\emptyset$, of 1.

Image-based small-scale 3-dimensional dosimetry was performed for one time point (4 hpi) to evaluate the intratumoral activity and dose rate distribution using α-camera imaging (*21*)of serial tumor tissue sections and voxel dose-point kernels, as described before(*22,23*).

Statistical analysis

Statistical differences were analyzed in GraphPad Prism (GraphPad software, Inc.) using the log-rank (Mantel-Cox) test for survival and linear regression for hematocrit.

RESULTS

Radioimmunoconjugate

After astatination, the immunoreactivity of the ^{211}At-MX35-F(ab')$_2$ was 85–95% and the radiochemical purity >95%.

Biodistribution and dosimetry

The separate study investigating the potential influence on tumor uptake from a prior α-RIT treatment showed no difference in uptake between tumors previously treated or not (Supplemental Fig. 1) and the values were in good agreement with those previously published (*15*). Hence, the tumor dose from repeat injections was calculated as the sum from all (1, 2 or 3) injections. The mean absorbed tumor dose was 4.2 Gy/MBq and the total tumor doses for all study groups, shown in Table 1, ranged from 0 to 16.4 Gy. The mean absorbed doses for all organs are shown in Table 2.

Tumor growth

The mean volume for all tumors at first treatment was 42 ± 28 (SD) mm^3. All treated mice had reduced tumor growth (Fig. 1) compared to the exponential growth of tumors on control mice. Groups receiving more than one fraction had the largest reduction. Overall, the tumor reduction was dose-dependent and initial reductions were followed by regrowth. In group 7 (Fig 1B), four tumors were surgically removed on day 54 due to size, shifting the mean growth curve downwards.

Complete eradication of all tumors was seen in groups 1 and 5, treated with the highest total injected activity (3.90 MBq and 2.96 MBq).

A TFF of 100% was found for tumor doses of 16.4 and 12.4 Gy, groups 1 and 5 (Table 1), respectively. At 9.5 Gy, group 2 had a TFF of 45%. A plot of TFF versus absorbed dose (Fig. 2) indicated a sigmoid dose-response. For comparison, a theoretical calculation of tumor control probability (TCP) was done, using the mean tumor volume at therapy and previously observed data (*24*) on OVCAR-3 cell diameter (13.3 ± 2.2 μm) and radiosensitivity (D_0: 0.56 Gy). For higher dose levels the experimental TFF was in good agreement with the theoretical TCP (dashed curve), while at lower dose levels the TFF was less steep indicating biological and dosimetric heterogeneity.

Blood

No obvious effect on hematocrit was seen at an early time interval (9–27 weeks) after treatment, but at a late interval (34–59 weeks) the mean values decreased linearly with increased activity (Fig. 3) and linear regression showed a slope significantly different from zero (P=0.0001). While the hematocrit (mean ± SD) for controls (groups 4, 8 and 12), were 57% ± 0.08%, 60% ± 0.08%, and 55% ± 0.04%, the groups treated with > 1MBq (3, 6 and 9) had values decreased to 50% ± 0.09%, 49% ± 0.06%, and 50% ± 0.04%, respectively. Group 2 (2.27 MBq) was the highest activity group with late survivors, and the hematocrit value (44%) could only be derived from one mouse.

WBC at 5–7 days after therapy was reduced to 70–80% of the values for controls, and then recovered. Ten to 12 days after the final α-RIT, the lower activity groups (6, 7, 9, 10 and 11) had recovered to

approximately 100%. Of these, one animal per group was used for long-term WBC and one year (37–49 weeks) after α-RIT, their relative WBC of 100% or more. In the higher activity groups (1, 2, 3, and 5) WBC had not recovered 10–12 days after the final administration and was 11%, 33%, 51%, and 65%, respectively. In these groups late-term WBC could not be analyzed.

Body weight

The weight progression for the highest activity groups receiving multiple administrations (Fig. 4, A and B) deviated from the controls relatively early (8–50 days). For groups receiving only one injection (Fig. 4 C), deviations from controls occur later (~250 days). The lowest weight progression was seen for the highest activity (3.90, 2.27, and 2.96 MBq) groups (1, 2, and 5, respectively) where many animals had to be sacrificed shortly after α-RIT.

Survival

The impact on survival from systemic effects of α-RIT was studied after the tumors were either surgically removed at the maximum allowed volume or having been eradicated by repeat α-RIT. Survival was studied up to 60 weeks (~400 days). A few animals had recurring tumor growth at the primary inoculation site after surgery. These were taken out of the study and censored in the survival analysis.

While undefined for most low-activity groups, the median survival (Table 1) for high-activity groups (above ~1 MBq)decreased linearly with increased total injected activity (Supplemental Fig. 2), from 44 weeks for group 9 (1.10 MBq) down to 11 and 16 weeks for groups 1 and 5 (3.90 and 2.96 MBq).

Figure 5 shows the Kaplan-Meier survival curves. For the groups receiving three fractions, statistical analysis by log-rank test showed that group 1 and 2, but not 3, were significantly different from their respective control (group 4). For the 2-fractions cohort, all treated groups were significantly different from the controls (group 8) and for single-fraction only the group given the highest activity (group 9).

DISCUSSION

We used a xenograft model to investigate the curative efficacy of fractionated systemic α-RIT on small solid tumors. While well suited for treatment of micrometastatic disease, we showed that TAT could also eradicate small solid tumor nodules. By fractionated α-RIT with high absorbed tumor doses was reached, accompanied with strong and dose-dependent antitumor effects. Complete remission (TFF=100%) was found for tumor doses of 12.4 and 16.4 Gy. At 9.5 Gy the TFF was 45%.

Most studies evaluating the antitumor efficacy of TAT have used micrometastatic models and tumor doses of 6–40 Gy have been reported for close-to or complete remission (*2,7,25-28*). The therapeutic potential of α-emitters for macroscopic tumors is sparsely investigated and the dose-levels required for tumor eradication are mostly unknown. A few studies have reported complete remission, at absorbed doses of 12–21 Gy (*14,29,30*). Other studies reported close-to, but not curative, antitumor effects (TFF:

60–95%) for doses of 9–28 Gy (*31-37*). The dose-levels found curative in the present study match rather well these reported. The biological effects per unit dose for the densely ionizing α-particles are generally considerably greater than those for electrons and β-particles and in the case of deterministic effects this difference can be accounted by the use of RBE. We have chosen to report absorbed dose in units of Gy, as recommended by the MIRD Committee (*38*). Assuming a RBE of 5(*15*), our doses of 12.4 and 16.4 Gy would correspond to 62 and 82 Gy, i.e. be in good agreement with the levels used in external beam therapy.

In this study, the total absorbed tumor dose was calculated as the sum of the dose from each fraction. This could introduce errors since the tumor uptake could be altered from prior treatment, e.g. through increased vasculature leakiness. However, when comparing untreated tumors with those previously treated, no difference in tumor uptake was observed (Supplemental Fig. 1). It could still be that the biological response of the tumors was altered by a prior therapy (i.e. a change in RBE), but the plot of TCP versus dose (Fig. 2) did not differ with the number of treatment factors. Therefore, the same absorbed dose factor (Gy/MBq) was used for all fractions. Although studies of biological effects from α-particles would gain from a dosimetry more detailed than mean absorbed dose to whole organs in most cases, we chose to evaluate the antitumor effects with respect to mean absorbed dose to whole tumor. Using TAT on solid tumors, antitumor effects may arise not only from irradiation of tumor cell but also from other targets, e.g. intratumoral vasculature (*25-27,39,40*). High-resolution α-camera imaging of the same tumor model as used here(*21*), showed clearly heterogeneous intratumoral activity distributions up to 7 hpi. Activity concentrations in stromal compartments were 5 times higher than the mean for the whole tumor and total absorbed dose to stroma and near-stroma tumor cells was two times higher than for other cells(*41*). In the present study, imaging at 4 hpi and initial 3D-dosimetry (*22*) showed that some tumor areas had a dose rate 10 times higher than the mean (Fig. 6). The absorbed dose rate and its' distribution has been shown to vary with time after injection in these macroscopic tumors (*21,22*) due to the temporal changes in intratumoral activity uptake and distribution. Besides the mean absorbed dose, the minimal absorbed tumor dose is of special interest and could be considered the limiting factor for antitumor efficacy. Preliminary data (*42*) from α-camera imaging at serial time points has shown that the minimal absorbed tumor dose was 30% lower than the mean. When comparing our TFF with a theoretical TCP, the experimental data disclosed a sigmoid, but shallower, dose-response curve (Figure 2). Such a slope is generally interpreted to represent biological and dosimetric heterogeneity and further supports the notion that the antitumor effects were not solely a question of dose-effect in each tumor cell. This indicates that irradiation of vascular compartments may play an important role in TAT of solid tumors and that improved methods for evaluating TAT will likely involve small-scale dosimetry to these and other targets.

This study was designed to maximize tumor dose, while avoiding acute bone marrow toxicity. Fraction scheme and activities were chosen to allow bone marrow recovery between the fractions. However, the administered activities were high and long-term toxicity effects (60 weeks) were clear. The median survival decreased linearly with total injected activity from 59 to 11 weeks. Toxicity was also seen by reduced body weight progression. WBC-analysis after α-RIT indicated bone marrow recovery for low activity groups, while for the high activity groups the reduction was close to acute myelotoxicity. A

decrease in hematocrit was seen at a late interval (34-59 weeks after therapy). The main external indication of poor health was dehydration and in some cases petechiae. The reasons for reduced long-term survival can only be speculated for but since we observed a linear decrease in median survival with increasing injected activity, we interpret the effects on survival as being due to systemic radiotoxicity. While myelotoxicity is a potential cause, as indicated by the WBC and hematocrit data, several organs had an absorbed dose above (bone marrow, thyroid, throat, lungs and kidneys) or close to (stomach, heart) their tolerance dose (calculated for 3 MBq and assuming a RBE of 5 for α-irradiation). We have initiated further studies to gain more knowledge of long-term toxicity after TAT regimens.

While TAT may be most promising for treatment of minimal disease, our findings show that α-emitters might prove useful also for solid tumors, provided that the normal tissue toxicity could be kept at acceptable levels. This could have clinical importance, since many of the patients recruited for TAT of minimal disease will likely have a range of tumor sizes, ranging from single cells to small solid nodules. Further improvements will likely involve new treatment modalities by which normal tissue toxicity could be reduced, as indicated for pretargeted α-RIT (*14,34*). A prerequisite for any treatment planning will, however, involve knowledge on the absorbed doses required for tumor eradication. With all the limitations for translating results derived experimentally in an animal model to the human situation, the results from the current study support further exploration of TAT for treating solid tumors.

CONCLUSION

We aimed at investigating if TAT, in addition to its promising role for treating micrometastatic and minimal disease, could be used to treat also macro tumors. Using intravenous fractionated α-RIT we found complete eradication for solid tumor xenografts receiving absorbed doses of 12.4 and 16.4 Gy. Hence, we conclude that TAT regimens could stretch beyond the realm of micrometastatic disease and be eradicative also for solid tumors. Our observations indicated that at least 10 Gy is required and this experimental finding was in good agreement with theoretical calculations of TCP. Considering a RBE of 5, this dose level seemed reasonable. However, complete remission was achieved first at activity levels close-to lethal and was accompanied with biological effects that reduced the long-term survival.

ACKNOWLEDGEMENTS

This work was supported by the Swedish Research Council, the Swedish Cancer Society, the King Gustaf V Jubilee Clinic Cancer Research Foundation and Assar Gabrielsson Cancer Research Foundation.

REFERENCES

1. Uusijarvi H, Bernhardt P, Ericsson T, Forssell-Aronsson E. Dosimetric characterization of radionuclides for systemic tumor therapy: influence of particle range, photon emission, and subcellular distribution. *Med Phys.* 2006;33:3260-3269.

2. Kennel SJ, Mirzadeh S. Vascular targeted radioimmunotherapy with 213Bi--an alpha-particle emitter. *Nucl Med Biol.* 1998;25:241-246.

3. Allen BJ, Tian Z, Rizvi SM, Li Y, Ranson M. Preclinical studies of targeted alpha therapy for breast cancer using 213Bi-labelled-plasminogen activator inhibitor type 2. *Br J Cancer.* 2003;88:944-950.

4. Michel RB, Rosario AV, Brechbiel MW, Jackson TJ, Goldenberg DM, Mattes MJ. Experimental therapy of disseminated B-Cell lymphoma xenografts with 213Bi-labeled anti-CD74. *Nucl Med Biol.* 2003;30:715-723.

5. Qu CF, Songl YJ, Rizvi SM, et al. In vivo and in vitro inhibition of pancreatic cancer growth by targeted alpha therapy using 213Bi-CHX.A"-C595. *Cancer Biol Ther.* 2005;4:848-853.

6. Beck R, Seidl C, Pfost B, et al. 213Bi-radioimmunotherapy defeats early-stage disseminated gastric cancer in nude mice. *Cancer Sci.* 2007;98:1215-1222.

7. Song H, Shahverdi K, Huso DL, et al. 213Bi (alpha-emitter)-antibody targeting of breast cancer metastases in the neu-N transgenic mouse model. *Cancer Res.* 2008;68:3873-3880.

8. Borchardt PE, Yuan RR, Miederer M, McDevitt MR, Scheinberg DA. Targeted actinium-225 in vivo generators for therapy of ovarian cancer. *Cancer Res.* 2003;63:5084-5090.

9. Andersson H, Elgqvist J, Horvath G, et al. Astatine-211-labeled antibodies for treatment of disseminated ovarian cancer: an overview of results in an ovarian tumor model. *Clin Cancer Res.* 2003;9:3914S-3921S.

10. Elgqvist J, Andersson H, Back T, et al. Alpha-radioimmunotherapy of intraperitoneally growing OVCAR-3 tumors of variable dimensions: outcome related to measured tumor size and mean absorbed dose. *J Nucl Med.* 2006;47:1342-1350.

11. Gustafsson AM, Back T, Elgqvist J, et al. Comparison of therapeutic efficacy and biodistribution of 213Bi- and 211At-labeled monoclonal antibody MX35 in an ovarian cancer model. *Nucl Med Biol.* 2012;39:15-22.

12. Hagan PL, Halpern SE, Dillman RO, et al. Tumor size: effect on monoclonal antibody uptake in tumor models. *J Nucl Med.* 1986;27:422-427.

13. Wang R, Coderre JA. A bystander effect in alpha-particle irradiations of human prostate tumor cells. *Radiat Res.* 2005;164:711-722.

14. Park SI, Shenoi J, Pagel JM, et al. Conventional and pretargeted radioimmunotherapy using bismuth-213 to target and treat non-Hodgkin lymphomas expressing CD20: a preclinical model toward optimal consolidation therapy to eradicate minimal residual disease. *Blood.* 2010;116:4231-4239.

15. Bäck T, Andersson H, Divgi CR, et al. 211At radioimmunotherapy of subcutaneous human ovarian cancer xenografts: evaluation of relative biologic effectiveness of an alpha-emitter in vivo. *J Nucl Med.* 2005;46:2061-2067.

16. Yin BW, Kiyamova R, Chua R, et al. Monoclonal antibody MX35 detects the membrane transporter NaPi2b (SLC34A2) in human carcinomas. *Cancer Immun.* 2008;8:3.

17. Lindegren S, Back T, Jensen HJ. Dry-distillation of astatine-211 from irradiated bismuth targets: a time-saving procedure with high recovery yields. *Appl Radiat Isot.* 2001;55:157-160.

18. Lindegren S, Frost S, Back T, Haglund E, Elgqvist J, Jensen H. Direct procedure for the production of 211At-labeled antibodies with an epsilon-lysyl-3-(trimethylstannyl)benzamide immunoconjugate. *J Nucl Med.* 2008;49:1537-1545.

19. Bäck T, Haraldsson B, Hultborn R, et al. Glomerular filtration rate after alpha-radioimmunotherapy with 211At-MX35-F(ab')2: a long-term study of renal function in nude mice. *Cancer Biother Radiopharm.* 2009;24:649-658.

20. Carlsson G, Gullberg B, Hafstrom L. Estimation of liver tumor volume using different formulas - an experimental study in rats. *J Cancer Res Clin Oncol.* 1983;105:20-23.

21. Bäck T, Jacobsson L. The alpha-camera: a quantitative digital autoradiography technique using a charge-coupled device for ex vivo high-resolution bioimaging of alpha-particles. *J Nucl Med.* 2010;51:1616-1623.

22. Bäck T, Chouin N, Lindegren S, Jensen H, Albertsson P, Palm S. Image-based small-scale 3D-dosimetry in targeted alpha therapy using voxel dose-point kernels and alpha camera imaging of serial tissue sections. *J NUCL MED MEETING ABSTRACTS.* 2014;55:50-.

23. Frost SH, Miller BW, Back TA, et al. alpha-Imaging Confirmed Efficient Targeting of CD45-Positive Cells After 211At-Radioimmunotherapy for Hematopoietic Cell Transplantation. *J Nucl Med.* 2015;56:1766-1773.

24. Palm S, Andersson H, Back T, et al. In vitro effects of free 211At,211At-albumin and 211At-monoclonal antibody compared to external photon irradiation on two human cancer cell lines. *Anticancer Res.* 2000;20:1005-1012.

25. Kennel SJ, Boll R, Stabin M, Schuller HM, Mirzadeh S. Radioimmunotherapy of micrometastases in lung with vascular targeted 213Bi. *Br J Cancer.* 1999;80:175-184.

26. Kennel SJ, Chappell LL, Dadachova K, et al. Evaluation of 225Ac for vascular targeted radioimmunotherapy of lung tumors. *Cancer Biother Radiopharm.* 2000;15:235-244.

27. Kennel SJ, Mirzadeh S, Eckelman WC, et al. Vascular-targeted radioimmunotherapy with the alpha-particle emitter 211At. *Radiat Res.* 2002;157:633-641.

28. Song H, Hobbs RF, Vajravelu R, et al. Radioimmunotherapy of breast cancer metastases with alpha-particle emitter 225Ac: comparing efficacy with 213Bi and 90Y. *Cancer Res.* 2009;69:8941-8948.

29. Petrich T, Quintanilla-Martinez L, Korkmaz Z, et al. Effective cancer therapy with the alpha-particle emitter [211At]astatine in a mouse model of genetically modified sodium/iodide symporter-expressing tumors. *Clin Cancer Res.* 2006;12:1342-1348.

30. Petrich T, Helmeke HJ, Meyer GJ, Knapp WH, Potter E. Establishment of radioactive astatine and iodine uptake in cancer cell lines expressing the human sodium/iodide symporter. *Eur J Nucl Med Mol Imaging.* 2002;29:842-854.

31. Behr TM, Behe M, Stabin MG, et al. High-linear energy transfer (LET) alpha versus low-LET beta emitters in radioimmunotherapy of solid tumors: therapeutic efficacy and dose-limiting toxicity of 213Bi- versus 90Y-labeled CO17-1A Fab' fragments in a human colonic cancer model. *Cancer Res.* 1999;59:2635-2643.

32. Norenberg JP. 213Bi-DOTA-Octreotide peptide receptor radionuclide therapy of pancreatic tumors in a preclinical animal model. Paper presented at: 8th International Symposium on Targeted Alpha Therapy, 2013; Oak Ridge.

33. Norenberg JP, Krenning BJ, Konings IR, et al. 213Bi-[DOTA0, Tyr3]octreotide peptide receptor radionuclide therapy of pancreatic tumors in a preclinical animal model. *Clin Cancer Res.* 2006;12:897-903.

34. Pagel JM, Kenoyer AL, Back T, et al. Anti-CD45 pretargeted radioimmunotherapy using bismuth-213: high rates of complete remission and long-term survival in a mouse myeloid leukemia xenograft model. *Blood.* 2011;118:703-711.

35. Wild D, Frischknecht M, Zhang H, et al. Alpha- versus beta-particle radiopeptide therapy in a human prostate cancer model (213Bi-DOTA-PESIN and 213Bi-AMBA versus 177Lu-DOTA-PESIN). *Cancer Res.* 2011;71:1009-1018.

36. Dahle J, Bruland OS, Larsen RH. Relative biologic effects of low-dose-rate alpha-emitting 227Th-rituximab and beta-emitting 90Y-tiuexetan-ibritumomab versus external beam X-radiation. *Int J Radiat Oncol Biol Phys.* 2008;72:186-192.

37. Dahle J, Borrebaek J, Jonasdottir TJ, et al. Targeted cancer therapy with a novel low-dose rate alpha-emitting radioimmunoconjugate. *Blood.* 2007;110:2049-2056.

38. Sgouros G, Roeske JC, McDevitt MR, et al. MIRD Pamphlet No. 22 (abridged): radiobiology and dosimetry of alpha-particle emitters for targeted radionuclide therapy. *J Nucl Med.* 2010;51:311-328.

39. Behling K, Maguire WF, Puebla JC, et al. Vascular targeted radioimmunotherapy for the treatment of glioblastoma. *J Nucl Med.* 2016;[Epub ahead of print].

40. Singh Jaggi J, Henke E, Seshan SV, et al. Selective alpha-particle mediated depletion of tumor vasculature with vascular normalization. *PLoS One.* 2007;2:e267.

41. Chouin N, Back T, Bardies M, et al. Statistical and dosimetric analysis of the penetration of antibody fragments F(ab')2 radiolabeled with 211At within subcutaneous tumors. *J NUCL MED MEETING ABSTRACTS.* 2011;52:75-.

42. Chouin N, Palm S, Lindegren S, Jensen H, Albertsson P, Back T. Intra-tumoral dose distributions after experimental targeted alpha therapy by Alpha-Camera imaging. *European Journal of Nuclear Medicine and Molecular Imaging.* 2014;41:151-705.

FIGURE 1. Mean Tumor growth after alpha-RIT

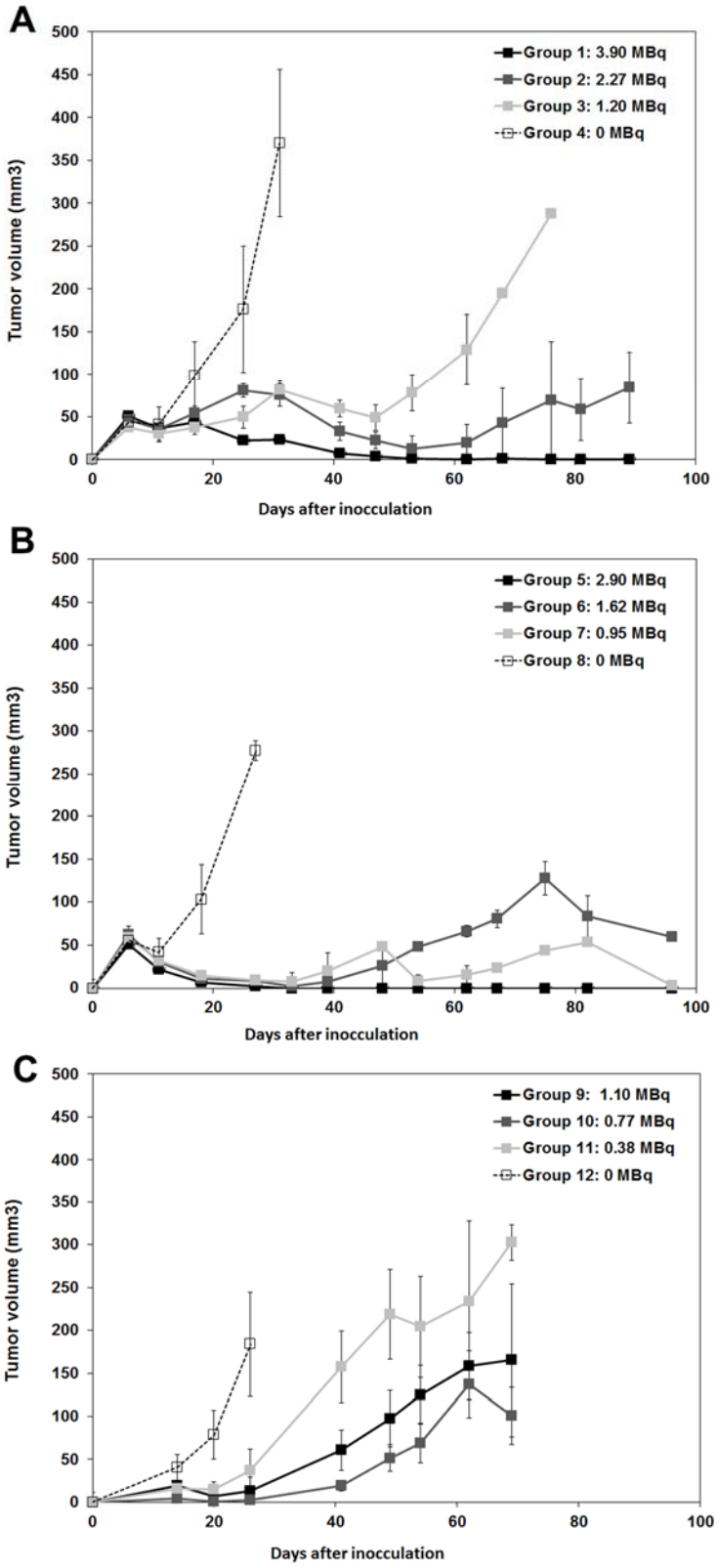

FIGURE 1. Tumor growth (mean ±SEM) after intravenous fractionated α-RIT with ^{211}At-MX35-F(ab')$_2$ plotted versus time after the first therapy (A: 3 fractions, B: 2 fractions, C: single fraction).

FIGURE 2 - TFF vs Tumor Dose

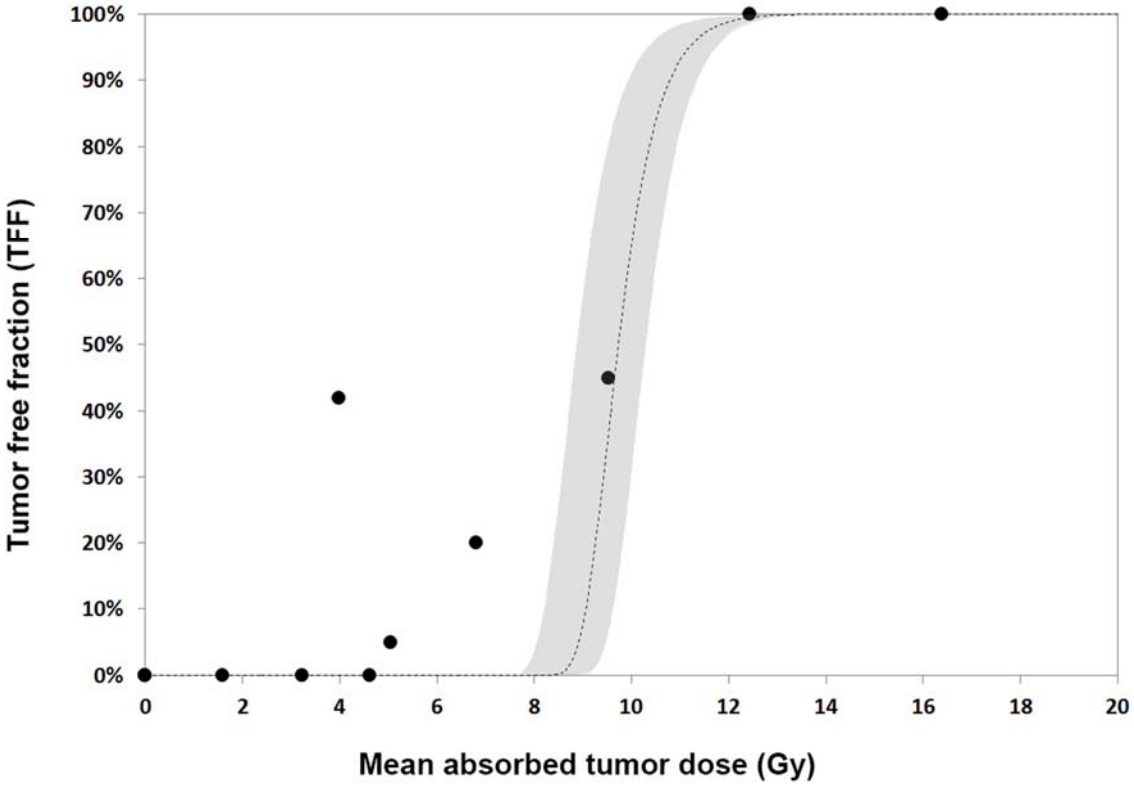

FIGURE 2. TFF plotted versus mean absorbed tumor. Dashed curves represent the theoretical TCP, calculated using the mean tumor volume (42 ± 28 mm^3) and previously observed data (*24*) on OVCAR-3 cell diameter (13.3 ± 2.2 μm) and radiosensitivity (D_0: 0.56 Gy). Grey area indicates a TCP-range calculated from assuming two different 'number of cells in a tumor' using the tumor volume [mean+1SD] and cell diameter [mean-1SD], or vice versa.

FIGURE 3 –Hematocrit after alpha-RIT

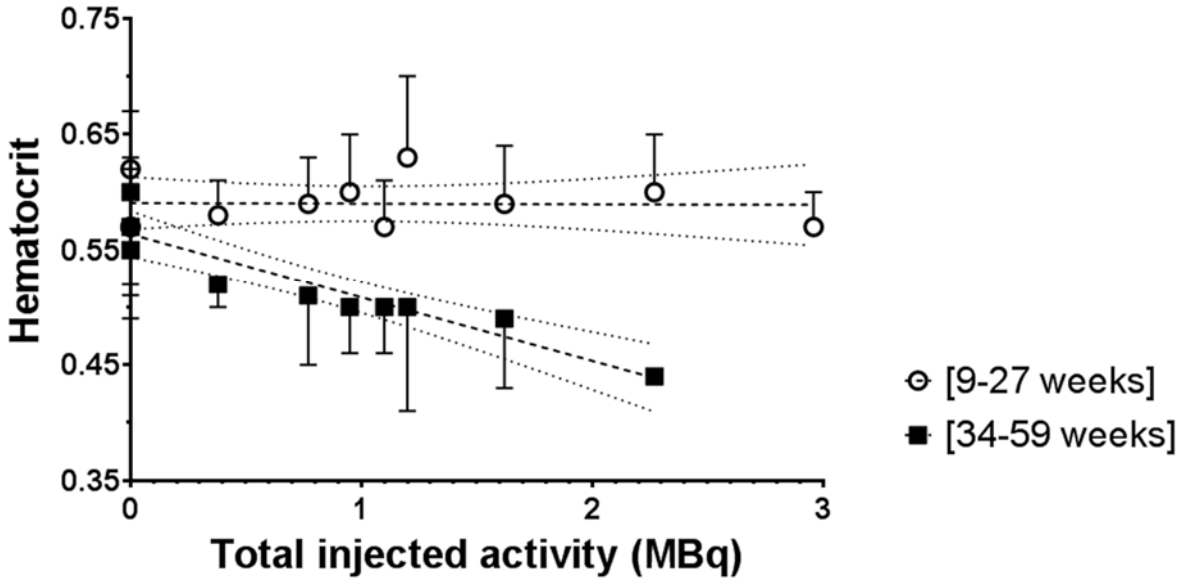

FIGURE 3. Hematocrit (mean ± SD) at an early (circles) and late (squares) time interval after α-RIT-injection, as a function of total injected activity. Dash lines indicate linear regression and 95% confidence interval.

FIGURE 4 – Body weight after alpha-RIT

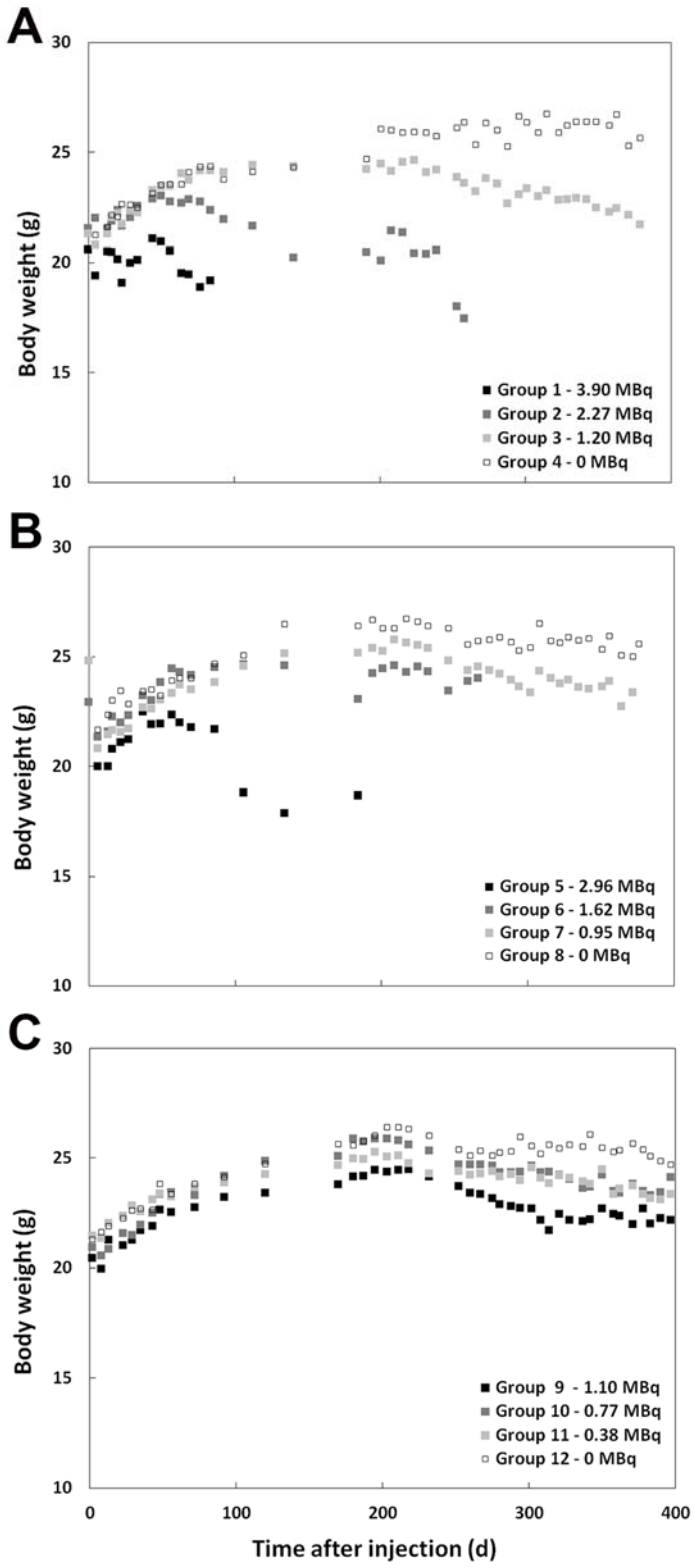

FIGURE 4. Mean body weights after first α-RIT-injection. (A) Groups receiving 3 fractions, (B) 2 fractions, and (C) one fraction.

FIGURE 5 – Survival plot after alpha-RIT

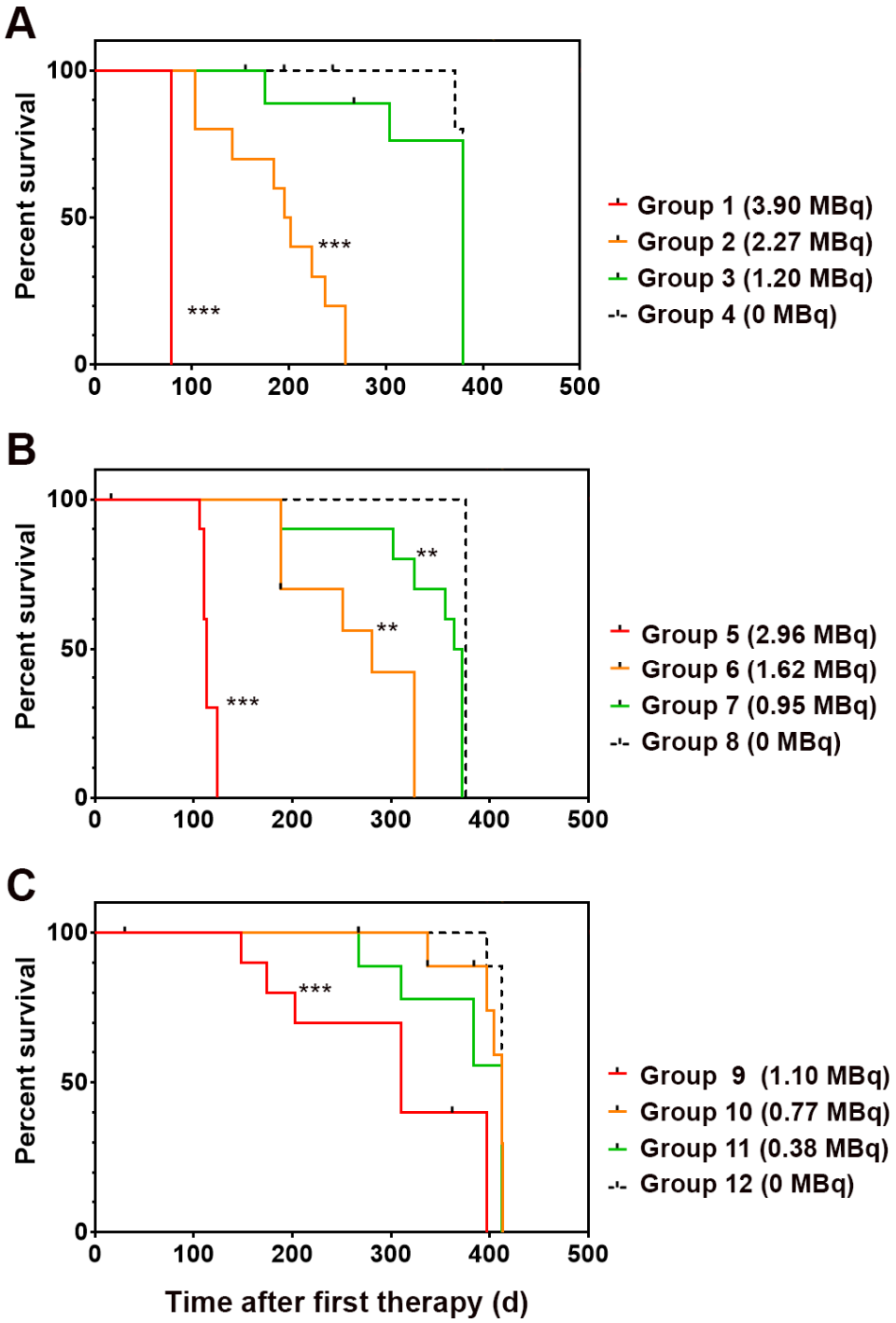

FIGURE 5. Percent survival as a function of time after first α-RIT-injection. N.B. All tumors remaining after the tumor growth monitoring period were surgically removed when exceeding 15 mm or at signs of ulcerated skin. The survival data therefore reflects other causes of death than progression of the primary subcutaneous tumors, e.g. systemic radiotoxicity of alpha-RIT. If tumor regrowth occurred a third time after surgery the animals were taken out of study and censored in survival analysis (tick marks). (A) 3 fractions, (B) 2 fractions, and (C) one fraction. Significant differences (treated versus respective controls) are indicated by **P<0.005 and ***P<0.0005.

FIGURE 6 – Intratumoral distribution by Alpha camera imaging

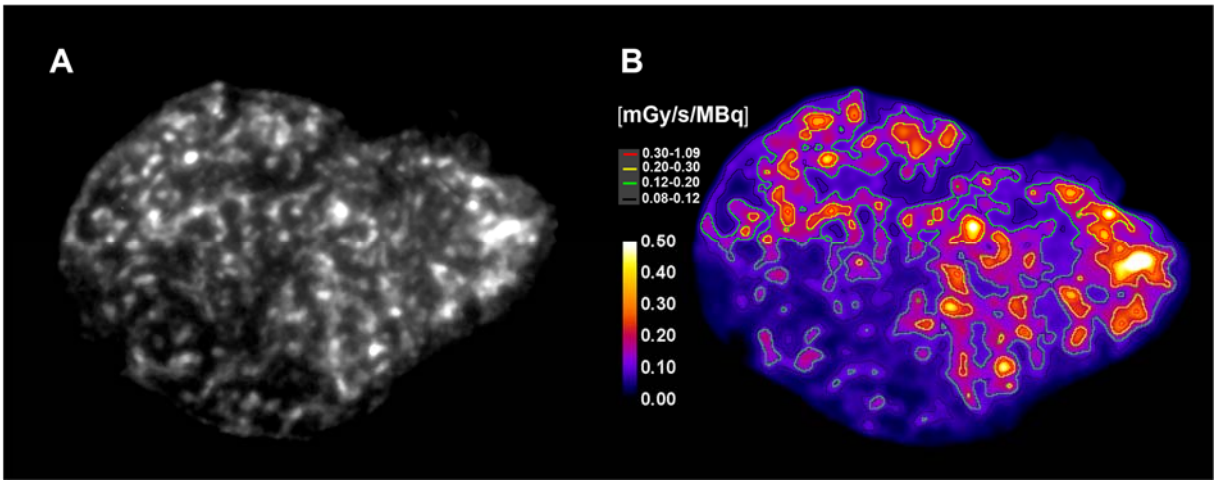

FIGURE 6. (A) Alpha Camera image of a OVCAR-3 sc-tumor 4 hpi after TAT in mice with At-211-MX35-F(Ab')$_2$. (B). Dose rate image with iso-dose curves for the selected dose intervals 0.08-0.12 (black), 0.12-0.20 (green), 0.20-0.30 (yellow) and 0.30-1.09 (red) mGy/s/MBq.

TABLE 1 – Study groups

Study group	No. of mice (tumors)	Injection 1 (MBq)	Injection 2 (MBq)	Injection 3 (MBq)	Total activity (MBq)	Median Survival (weeks)	Total absorbed tumor dose (Gy)	TFF
1	10(20)	1.34	1.46	1.10	3.90	11	16.4	100%
2	10(20)	0.87	0.63	0.77	2.27	28	9.5	45%
3	10(20)	0.36	0.46	0.38	1.20	*N.D.*	5.0	5%
4	8(15)	0.00	0.00	0.00	0.00	*N.D.*	0.0	0%
5	10(20)	1.53	1.43	-	2.96	16	12.4	100%
6	10(20)	1.02	0.60	-	1.62	40	6.8	20%
7	10(17)	0.50	0.45	-	0.95	*N.D.*	4.0	42%
8	10(20)	0.00	0.00	-	0.00	*N.D.*	0.0	0%
9	10(20)	1.10	-	-	1.10	44	4.6	0%
10	10(20)	0.77	-	-	0.77	*N.D.*	3.2	0%
11	10(20)	0.38	-	-	0.38	*N.D.*	1.6	0%
12	10(20)	0.00	-	-	0.00	*N.D.*	0.0	0%

TABLE 1. Tumor free fraction (TFF) was calculated at 81–84 days after tumor inoculation for treated groups and at 39–41 days for the control groups.

TABLE 2 – Organ absorbed doses

Organ	Mean absorbed dose (Gy/MBq)
Blood	5.0
Bone marrow*	2.0
Salivary glands	2.8
Throat	11
Thyroid †	45
Lung	3.4
Heart	2.0
Stomach	2.8
Small Intestine	1.2
Large intestine	0.8
Liver	1.2
Spleen	1.5
Kidney	4.0
i.p. fat	0.8
Muscle	0.4
Tumor	4.2

TABLE 2. Mean absorbed organ doses. *Dose to red bone marrow was estimated using a bone marrow-to-blood-ratio of 0.35. † Dose to thyroid was estimated from throat content assuming that all activity was located in thyroid and using a standard weight of 3 mg.

SUPPL. FIGURE 1 – Effect of previous alpha-RIT on tumor uptake

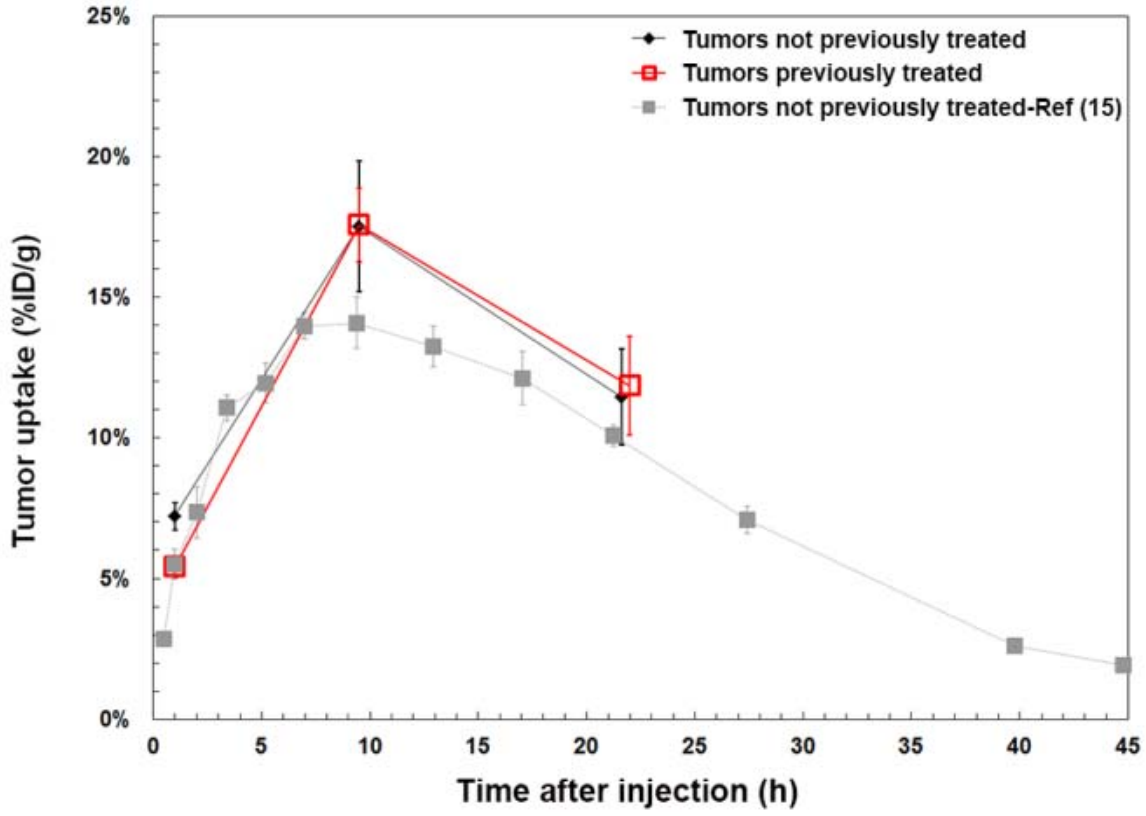

Suppl. Figure 1. Comparison of the tumor uptake for tumors not being treated before with the uptake of tumors having received a prior α-RIT treatment. Tumor uptake (%IA/g) is plotted versus time after injection. Grey curve shows tumor uptake from a previous biodistribution study (*15*).

SUPPL. FIGURE 2

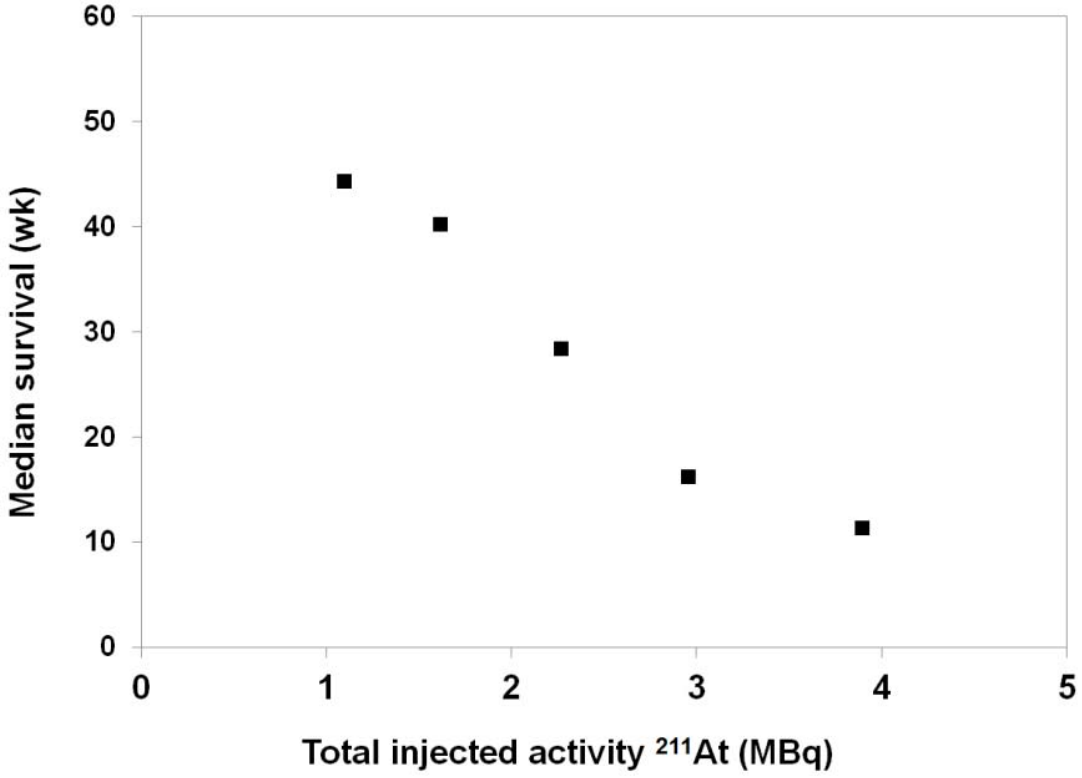

Suppl. Figure 2. Median survival as a function of total injected activity (sum all fractions). Groups with undefined median survival (alive at study termination) are excluded. All tumors remaining after the tumor-growth monitor period were surgically removed when exceeding 15 mm or at signs of ulcerated skin. The survival data therefore reflects other causes of death than progression of the primary subcutaneous tumors, e.g. systemic radiotoxicity of alpha-RIT.